Molecular Simulation
Vol. 35, Nos. 10–11, September 2009, 953–961

Taylor & Francis
Taylor & Francis Group

Exploring gas permeability of lipid membranes using coarse-grained molecular dynamics

Huajun Yuan, Cynthia J. Jameson and Sohail Murad*

Department of Chemical Engineering, University of Illinois at Chicago, 810 S. Clinton, Chicago, IL 60607, USA

(*Received 10 December 2008; final version received 18 January 2009*)

Molecular transport through biological membranes occurs in a range of interesting processes. To understand basic permeation functions of a biomembrane, we have carried out molecular dynamics (MD) simulations using dipalmitoylphosphatidylcholine (DPPC) as the bilayer membrane. By reducing the degrees of freedom and employing suitable potentials, a coarse-grained (CG) model can provide direct insight into collective phenomena in biological membranes at longer time and length scales. We used a CG model for DPPC bilayer, which had been parametrised to mimic fundamental structural properties. The permeation process of small molecules such as Xe, O_2 and CO_2 through the lipid bilayers was investigated. The density profiles and the local diffusion coefficients of the permeating gases across the bilayer membranes are obtained from the MD simulations. By studying gas molecules permeating through the lipid bilayer, we obtain an improved understanding of transport processes across membranes in biological systems in the absence of specialised channels. We also explore conditions that will give better control of the gas permeability and the possibility of membrane applications in environment-friendly separation processes.

Keywords: coarse grain; gas; permeability; lipid membrane

1. Introduction

Transport of chemical species across membranes is of significance in separations, sensors, pharmacological applications and life itself. Many biological processes involve transport of molecules through membranes. Under various conditions, molecules can permeate through a biomembrane following different mechanisms, some of which are very complex [1]. It is important to understand the mechanism and basic permeation functions of biomembranes, not only for better design of environment-friendly separation processes but also for designing drug delivery systems.

Lipid bilayers are one of the major structural elements of biological membranes, which play a key role for other species such as proteins to function. For ions and charged molecules, the lipid bilayer is essentially almost impermeable, but small neutral molecules such as water, oxygen and carbon dioxide can permeate through at significant rates, without the help from proteins. Since the permeation of small molecules through lipid bilayers is still not completely understood, it is of significant importance to gain some insights into the permeation process, which will enhance the understanding of membranes in general and their interactions with small molecules in particular. Even in the presence of channels, the major route of water permeation through plasma membranes still seems to be through the lipid bilayer [2].

Experimental permeation rates of small molecules can be measured by means of osmotic, nuclear magnetic resonance (NMR) and radio-tracer experiments, although the interpretation of the results is often difficult [3]. The large spread in reported permeation rates is mainly caused by unstirred layer effects and differences in the estimates of membrane area and volume. Paula et al. [4] measured the permeability coefficient of potassium ions and small polar molecules as a function of membrane thickness. Jansen and Blume [5] compared diffusive and osmotic water permeation across phospholipid bilayers with different head groups and fatty acyl chains. Overall, the permeability is affected by the characteristic properties of the small molecules, such as size, hydrophobicity and shape, and properties of the lipid membrane, such as the number/size of head groups, chain length, chain branching, and whether the chain is saturated or unsaturated.

Simulations using molecular dynamics (MD) are a powerful tool, providing structural and dynamic details of the permeation which are not easily obtained from experiments. Marrink and Berendsen [6] used the MD method to calculate the permeability coefficients of water and some small molecules and proposed the inhomogeneous solubility–diffusion model. Recently, progress has been reported on investigations of the permeability of small uncharged molecules across lipid bilayers based on this model [7–10]. These authors used MD simulation methods at the atomistic or united atom level to study the local diffusion coefficient of a range of small gas molecules inside the lipid membrane and have examined the role of solute and lipid molecules on the permeability.

*Corresponding author. Email: murad@uic.edu

ISSN 0892-7022 print/ISSN 1029-0435 online

DOI: 10.1080/08927020902763839
http://www.informaworld.com

Although atomistic simulations are now able to reproduce and predict many fundamental properties of lipid membranes, the size of systems and time scale of phenomena are still limited by current computers and algorithms. On the other hand, coarse-grained (CG) models, in which one treats small groups of atoms as single particles, provide a promising approach to increase the time scale of biomolecular simulations [11]. There is a large variety of CG approaches available, ranging from qualitative solvent-free models to models that include chemical specificity. Marrink and co-workers [12–14] recently developed a CG force field called MARTINI parametrised specifically for simulation of lipids and surfactants. This force field has been shown to semi-quantitatively reproduce fundamental structural and thermodynamic properties of lipid bilayers.

In this study, we have used a CG model to investigate the gas permeation process through lipid bilayers. Instead of aiming for a complete analysis, we have attempted to gain a basic insight of the mechanism through which the gas molecules permeate the lipid membranes. The goal of this study is to gain semi-quantitative insights into the gas permeation process across lipid bilayers. The effects of the hydrocarbon chain length of lipid molecules on the permeation process were investigated using three types of lipid membranes: dicapryloylphosphatidylcholine (DCPC), dimyristoylphosphatidylcholine (DMPC) and dipalmitoylphosphatidylcholine (DPPC). We investigated the permeability of three small molecules, xenon, oxygen and carbon dioxide, through the lipid bilayers using MD with the CG MARTINI force field for the lipid bilayer. We have also compared the simulation results with available experimental results. We tested other force fields such as those developed by the Klein group [15], but were unable to reproduce the correct structural details of the membranes. Other researchers [16] studying lipid membranes have also been able to use the MARTINI force field with similar success.

2. Methods

2.1 Lipid structures

We performed MD simulations in three saturated lipid bilayer systems with different hydrocarbon chain lengths: DCPC (C_8), DMPC (C_{14}) and DPPC (C_{16}). The molecular structures of these are shown in Figure 1.

2.2 Models

The MARTINI CG force field is based on a four-to-one mapping, i.e., on average, four heavy atoms are represented by a single interaction site [14]. We will only briefly summarise it here, since details have been previously published [13]. The model considers four main types of interaction sites: polar (P), nonpolar (N), apolar (C) and charged (Q). Within a main type, subtypes are distinguished either by a letter denoting the hydrogen-bonding capabilities

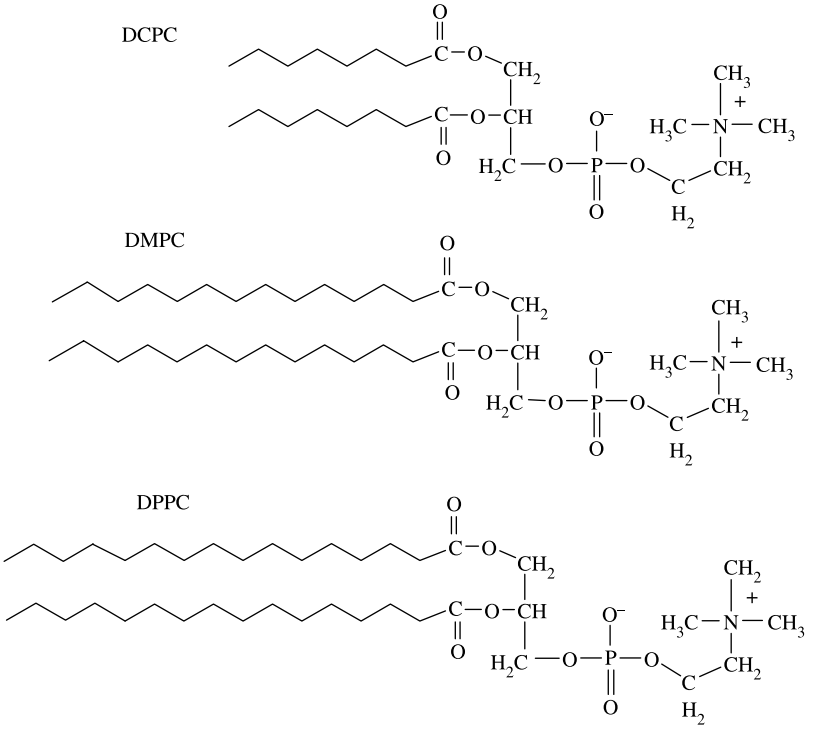

Figure 1. Molecular structures of DCPC (C_8), DMPC (C_{14}) and DPPC (C_{16}).

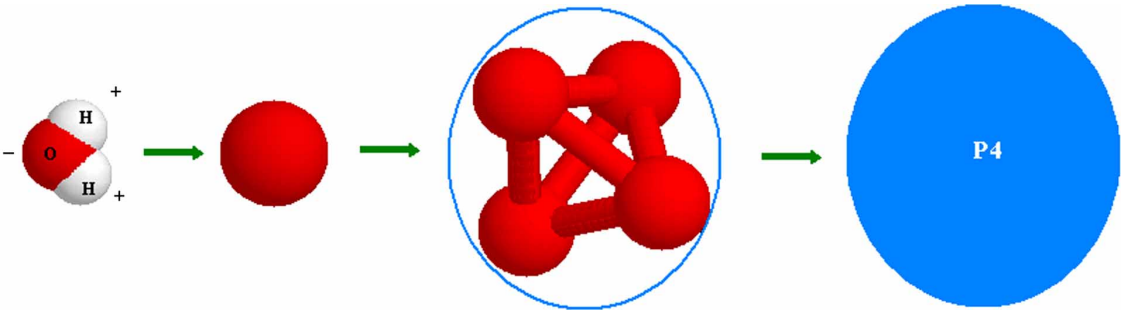

Figure 2. Coarse-grained mapping strategy for water.

(d, donor; a, acceptor; da, both; o, non) or by a number indicating the degree of polarity (from 1 = lower polarity to 5 = higher polarity). The mapping of a CG water site (P_4) is shown in Figure 2.

For the lipids, the same mapping strategy is applied, the phospholipid DPPC is modelled using 12 CG sites; DMPC and DCPC are modelled by removing one and two tail beads from each tail, respectively. The mapping strategy of a DMPC molecule is shown in Figure 3.

All particle pairs i and j at distance r_{ij} interact via a Lennard-Jones (LJ) potential:

$$V_{\mathrm{LJ}}(r_{ij}) = 4\varepsilon_{ij}\left[\left(\frac{\sigma_{ij}}{r_{ij}}\right)^{12} - \left(\frac{\sigma_{ij}}{r_{ij}}\right)^{6}\right]. \quad (1)$$

The well depth ε_{ij} depends on the interacting particle types and values range from $\varepsilon_{ij} = 5.6$ kJ/mol for interactions between strong polar groups to $\varepsilon_{ij} = 2.0$ kJ/mol for interactions between polar and apolar groups mimicking the hydrophobic effect. The effective size of particles is governed by the LJ parameter $\sigma = 0.47$ nm for all normal particle types, except that for interaction between charged (Q type) and most apolar types (C1 and C2), the range of repulsion is extended by setting $\sigma = 0.62$ nm. In addition to LJ interaction, charged groups interact via a shifted Coulombic potential function:

$$U_{\mathrm{elec}} = \frac{q_i q_j}{4\pi\varepsilon_0\varepsilon_r r}. \quad (2)$$

In the simulations, the nonbonded interactions are cut off at $r_{\mathrm{cut}} = 1.2$ nm. The LJ potential is shifted from $r_{\mathrm{shift}} = 0.9$ to 1.2 nm and the electrostatic potential is shifted from $r_{\mathrm{shift}} = 0.0$ to 1.2 nm following a standard shift function [17].

The bonds are described by a harmonic potential $V_{\mathrm{bond}}(R)$

$$V_{\mathrm{bond}}(R) = \frac{1}{2}K_{\mathrm{bond}}(R - R_{\mathrm{bond}})^2 \quad (3)$$

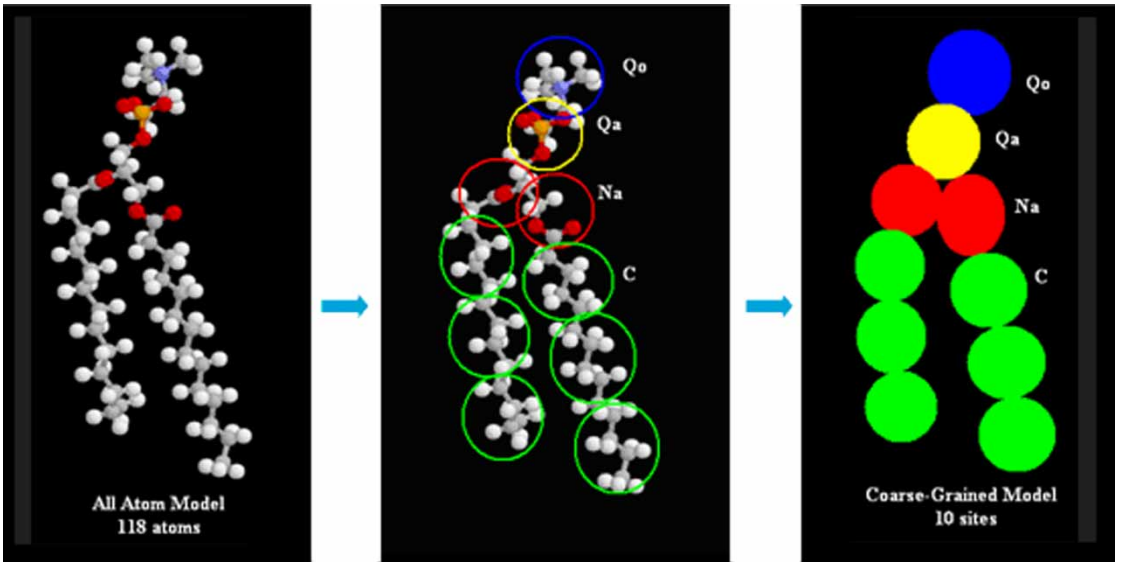

Figure 3. Coarse-grained mapping strategy for a DMPC molecule.

Table 1. Potential parameters of gas molecules studied.

Molecule	Interaction sites	σ(Å)	ε(K)	Q (e)	r_{bond} (Å)
O_2 [18]	Central LJ	3.36	120	0	
Xe [19]	Central LJ	3.9478	228	0	
CO_2 [20]	C	2.757	28.129	0.6512	1.149
	O	3.033	80.507	−0.3256	

and a cosine-type harmonic potential $V_{angle}(\theta)$ is used for bond angles.

$$V_{angle}(\theta) = \frac{1}{2} K_{angle}\{\cos(\theta) - \cos(\theta_0)\}^2. \quad (4)$$

The gas molecules we investigated include xenon, oxygen and carbon dioxide. In the case of xenon and oxygen since the electrostatic interactions are relatively weak, and the permeation rate would be primarily sterically driven, we chose a central LJ model. In the case of CO_2, because of the importance of the electrostatic interactions, we chose a three-centred model with point charges. The potential parameters used for these molecules are listed in Table 1.

For the cross-interactions between gas sites and lipid/water sites, we have used the Lorentz–Berthelot mixing rule as a starting point in this study, and we may modify the interaction parameters in the future to obtain a better description of the interactions [21].

2.3 *Calculation of permeability*

Using a conventional solubility–diffusion model and considering the complexity of lipid bilayers, Marrink and Berendsen [2,6] have proposed the inhomogeneous solubility–diffusion model. In this model, the permeability coefficient P can be calculated by the following equation:

$$\frac{1}{P} = \int_{z_1}^{z_2} R(Z)\mathrm{d}Z = \int_{z_1}^{z_2} \frac{\exp\{\Delta G(Z)/k_B T\}}{D_z(Z)}\mathrm{d}Z. \quad (5)$$

Here, Z_1 and Z_2 represent the z-coordinates of the two sides of the bulk aqueous phase, $R(Z)$ is defined as the local resistance to permeation, $\Delta G(Z)$ and $D_z(Z)$ are the excess free energy and the local diffusion coefficient of a small molecule permeating the membrane, k_B is the Boltzmann constant, and T is the temperature.

As an alternative to the solubility–diffusion mechanism, Jansen and Blume [5] have proposed the transient pore mechanism, which suggests that the transport of water molecules largely occurs across a transient pore in the lipid bilayer. The real mechanism of permeation of small molecules across a lipid bilayer is still not clearly understood and the experimental results are often different and sometimes inconsistent with each other [4].

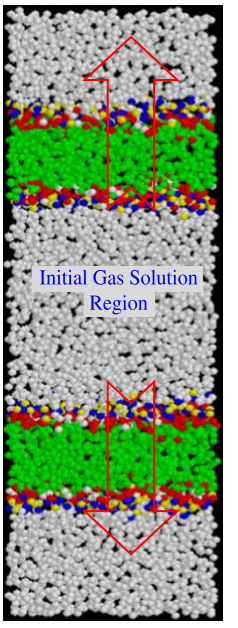

Figure 4. Simulation system for gas permeability measurement (DMPC).

Our approach for examining permeation closely replicates a real experiment. Previously reported simulation studies began with gas molecules on both sides of a single lipid layer [10] or else in the hydrophobic inner section of the lipid membrane [12]. We instead designed a system with two bilayers separated by aqueous phases ('inside' and 'outside') and with gas molecules introduced in the aqueous middle compartment formed by the two layers, as shown in Figure 4. The gas molecules can therefore only permeate from 'inside' to 'outside' at the onset of the simulation. By monitoring changes in the density profile, we then measure the diffusion coefficient of the gas through the membrane until the gas concentration gradient has diminished to nearly 0, which is a sign of equilibrium, with a net flux across the bilayer of 0. To enable comparisons with experimental measurements, we also introduce a definition of gas permeability as follows [22]:

$$P = \frac{D_\perp}{D_{//}}. \quad (6)$$

Here,

$$D_\perp = D_z = \frac{1}{2\times 1}\lim_{t\to\infty}\frac{\langle|r(t) - r(0)|^2\rangle_z}{t}, \quad (7)$$

and

$$D_{//} = D_{x+y} = \frac{1}{2\times 2}\lim_{t\to\infty}\frac{\langle|r(t) - r(0)|^2\rangle_{x+y}}{t}. \quad (8)$$

If the membrane is absolutely impermeable, the ratio of $D_{\perp}/D_{//}$ will be 0. On the other hand, if the gas molecule can permeate freely through the membrane, the ratio will be 1. Usually the permeability will be between 0 and 1, and our previous work [23] has shown that this definition is qualitatively very comparable with the experimental measurements.

By using this definition of permeability, we can compare our simulation results directly with the experimental results without additional concerns about the conversion of the CG time scales to real time, a well-known problem in CG simulations [13]. It has otherwise been suggested that a scale factor of four is usually needed at this level of coarse graining in order to compare with the experimental results [12]. For diffusion constants, the CG model results are 2- to 10-fold larger in comparison with the atomistic simulations [24].

2.4 *MD simulations*

We performed molecular dynamic simulations in three saturated lipid bilayer systems with different tail lengths: DCPC (C_8), DMPC (C_{14}) and DPPC (C_{16}). All the simulations were performed with the LAMMPS simulation package [25]. The dynamics are faster than that for fully atomistic simulations because the CG interactions are much smoother compared with atomistic interactions. For better stability, we used a smaller time step of 20 fs. Each system studied consists of 256 lipid molecules and 4000 water molecules forming two layers of lipid bilayers, as shown in Figure 4. In our simulations, we monitored the self-assembly of the bilayer first. When the system approached equilibrium at 323 K in the NPT ensemble, we checked the thickness of the CG DPPC lipid bilayer. This is measured from the peaks of the phosphate distribution, and found to be 3.75 nm, close to the experimental value of 3.85 nm [26]. After equilibration, we introduced a specific number of gas molecules into the aqueous phase between the two lipid bilayers to observe the unidirectional permeation (from inside to outside). We used the Nose–Hoover chain method for the NVT simulation [27,28]. The density profile of the gas and the mean square displacements (MSD) of the gas molecules can then be measured as the system evolves towards equilibrium. Tests were performed to ensure that the CG model can reproduce the experimental bulk properties of the species and also reproduce previous atomistic simulation results, the calculated area per lipid for DPPC at 323 K is 63.1 $Å^2$, which matches the experimental estimation of 64 $Å^2$ [26].

3. Results and discussions

3.1 *Permeation of gases*

The first gas studied was xenon at a temperature 323 K in DPPC–water system. Xenon atoms in the ground state are spherical, with high electric dipole polarizability that enhances dispersion forces. Because of its simple atomic structure, xenon has been extensively used to study gas solubilities in organic liquids [29,30]. After the DPPC–water system is equilibrated, eight xenon atoms were placed in the middle compartment of the system. We chose a small number of gas molecules, since the solubility of xenon in water is rather low. This avoids the situation where the pressure in the middle compartment becomes large and affects the stability of the lipid bilayer membranes. The density profiles of xenon, water and lipids obtained in a typical simulation are shown in Figure 5 after a shorter simulation of 10 ns and longer simulation of 100 ns. The triangles are water atoms and the squares are lipid atoms, the diamonds are xenon atoms. The density profile of bulk water is quite uniform while the density profile of lipid shows peaks

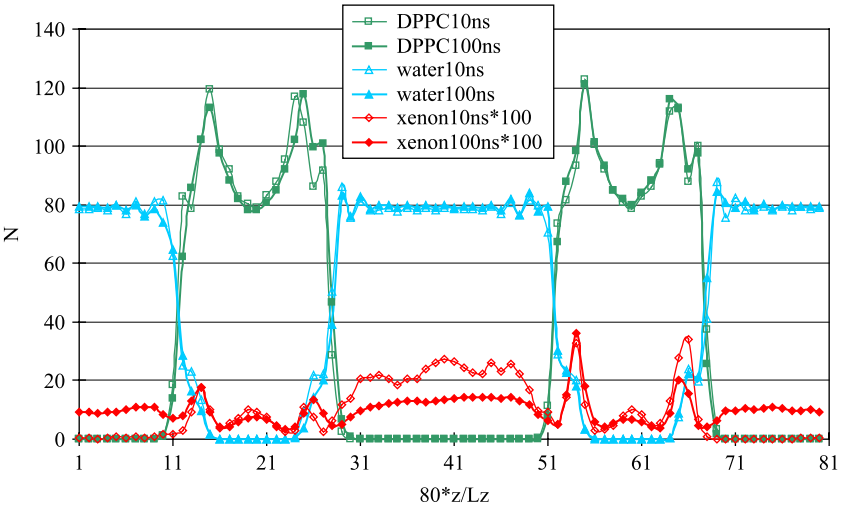

Figure 5. Density profile of xenon in DPPC–water simulation system.

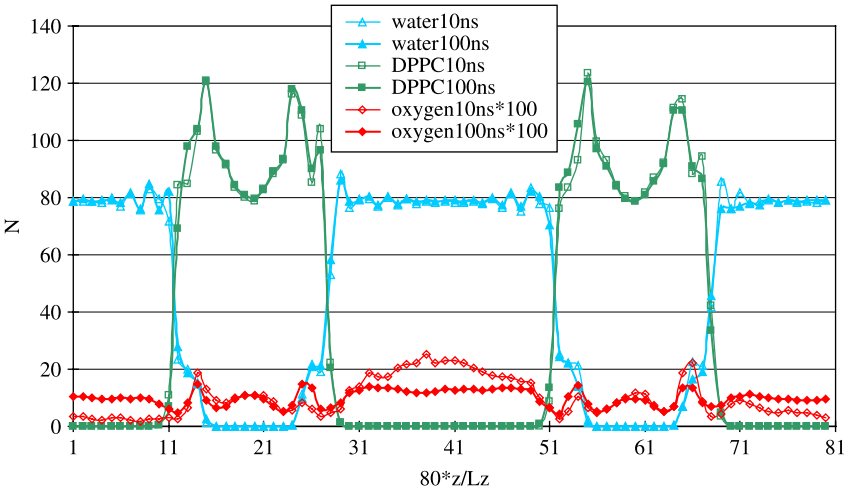

Figure 6. Density profile of oxygen in DPPC–water simulation system.

at the lipid/water interface. We found similar behaviour in the gas density profiles that showed the peaks near the gas–membrane interface [29].

From Figure 5, we can see that at 10 ns, the xenon has started to permeate through the lipid bilayer. The xenon density outside is low and the xenon atoms are starting to exit the membrane. Between 10 and 100 ns, the xenon continues permeating across the lipid bilayer and finally after 100 ns the system approaches equilibrium; the inside and outside density profiles become almost uniform.

For oxygen in DPPC–water system, the changes in the density profiles follow the same trend, and are shown in Figure 6. Comparing the density profiles of xenon and oxygen at 10 ns in Figures 5 and 6, we can see that the oxygen molecules permeate the lipid bilayer faster than the xenon. This is not surprising since we use a single site model for oxygen, just as for xenon. With a smaller particle size, it is easier for the oxygen molecule to permeate through the membrane than xenon.

For studies with carbon dioxide, we used the fully flexible Harris EPM2 model [20]. Our results are somewhat surprising since we found that carbon dioxide molecules could not enter the lipid bilayer at all, irrespective of how long we ran the simulation. The carbon dioxide molecules seemed stuck in the lipid/water interface and did not penetrate the lipid bilayer, as shown in Figure 7.

Others who have studied carbon dioxide reported permeation through the lipid bilayer, in both atomistic simulations [10] and experiments [31–33], although the reported carbon dioxide permeability across an EYPC/cholesterol bilayer experiment measured experimentally by Gutknecht et al. [34] is rather small. Our results that show no permeation are very likely caused by the three-centre potential model for the carbon dioxide molecule not being compatible with the intermolecular potential used

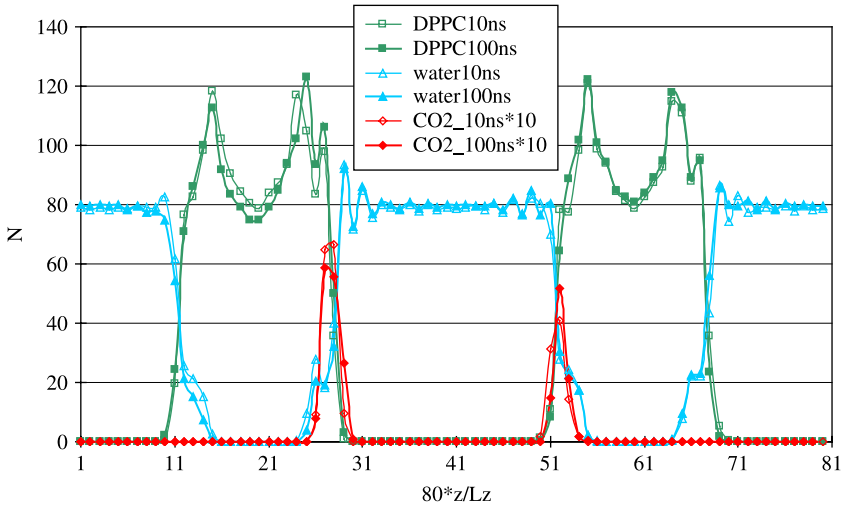

Figure 7. Density profile of carbon dioxide in DPPC–water simulation system.

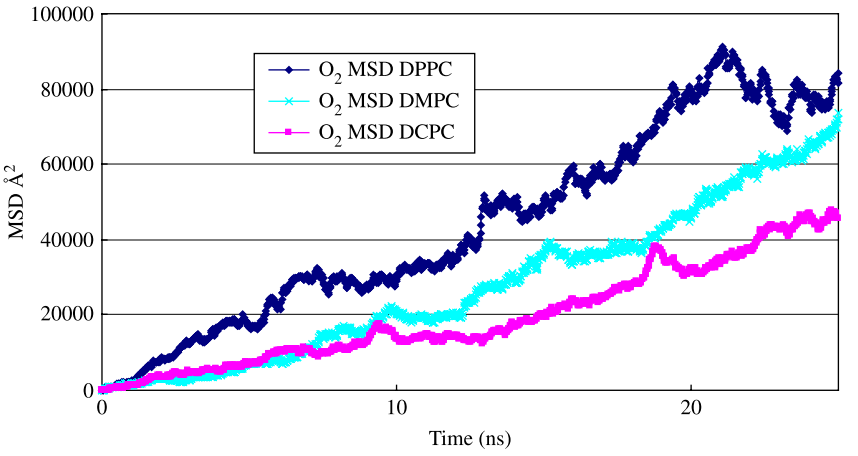

Figure 8. MSD curve of oxygen in different simulation systems.

for highly CG lipid and water. The Coulombic forces between the charged carbon and oxygen atoms of carbon dioxide and the head groups of the lipid molecules lead to very strong adsorption at the lipid heads. It therefore appears that when an atomistic CO_2 model is used, a more detailed/atomistic model for the lipids/water would be needed for compatibility than the CG model used here.

3.2 *Calculation of permeability of gases*

We first calculated the diffusion coefficient from MSD of the gas molecules. The slope of the MSD curve is proportional to the diffusion coefficient [35]. For three-dimensional diffusion, the diffusion coefficient can be expressed as:

$$D = \frac{1}{2\times 3}\lim_{t\to\infty}\frac{\langle|r(t)-r(0)|^2\rangle}{t}. \qquad (9)$$

The MSD curves of oxygen in three lipids for 25 ns are shown in Figure 8; permeation begins to be observed during this time period.

Diffusion coefficients can be calculated easily from these curves but unfortunately do not provide useful information on the permeation process. In addition, since gas molecules pass through the various phases, bulk water and the lipid bilayer, the calculated D is, in any case, only an effective diffusion coefficient. The calculated diffusion coefficients of oxygen in DPPC–water, DMPC–water and DCPC–water were found to be 5.86 ± 0.64, 3.93 ± 0.41, 2.68 ± 0.32 × 10^{-9} m^2/s, respectively. Xenon diffusion coefficients in these three systems were also calculated and the results are listed in Table 2. Both Xe and O_2 molecules exhibit diffusion coefficients that systematically depend on the lipid tail lengths.

Direct measurement of diffusion rates of small molecules within the membrane by experiments is very difficult [6]. From fluorescence measurements, a value of $D = 1.54 \times 10^{-5}$ cm^2/s was derived for oxygen diffusion across the DPPC membranes in a liquid crystalline phase at $T = 318$ K by Fishkoff et al. [36]. If we rescale our simulation results for effective diffusion coefficient of oxygen in DPPC at 323 K, by the usual factor of four [12], considering the time scale of CG simulations, our simulation results give an effective oxygen diffusion coefficient of $D = 1.47 \times 10^{-9}$ m^2/s. The agreement with value derived from the fluorescence experiments is quite reasonable, but considering experimental and simulation force field uncertainties, CG time conversion may not be a sensitive test of our simulation.

A more meaningful comparison with experimental studies is possible with permeability as defined in Equation (6): the ratio of diffusion coefficients in the z direction (perpendicular to the membrane surface) to diffusion coefficient in the xy plane (parallel). The MSD curves for the first 10 ns shown in Figure 9 can be used to calculate the permeability using Equations (6)–(8). We would like to point out that as stated previously the results reported include molecules both inside and outside the lipid bilayer. Since the fraction in these two phases can vary at different times, the results have more scatter than that would be observed in single-phase mean-squared displacement plots. However, our main interest in the ratio of the two diffusion rates, which will be similarly affected.

The permeability of oxygen through DPPC membrane thus obtained for oxygen is 0.775 ± 0.11; and for xenon it is 0.334 ± 0.06. Subczynski et al. [31] have reported an experiment to measure permeability of oxygen through

Table 2. Diffusion coefficients of gas in different lipid systems.

	O_2	Xe
Effective diffusion coefficient D (10^{-9} m^2/s)		
DPPC[C_8] + water	5.86 ± 0.64	2.4 ± 0.26
DMPC[C_{14}] + water	3.93 ± 0.41	1.43 ± 0.14
DCPC[C_{16}] + water	2.68 ± 0.32	1.02 ± 0.11

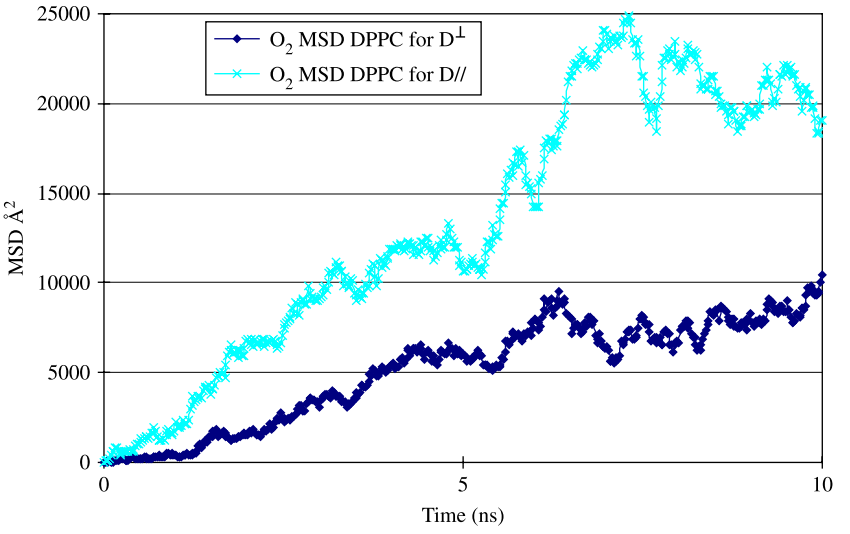

Figure 9. MSD curves of oxygen in DPPC simulation systems.

a Chinese hamster ovary plasma membrane using spin-labelled stearic acid. Spin labels were synthesised into the hydrocarbon tail of stearic acid at one of three locations: at the end, in the middle, or near the head. A very low concentration of these spin-labelled stearic acid molecules were intercalated within the membrane. By measuring the relaxation time change of the spin labels in the lipid bilayer portion of the membrane, the collision rate of oxygen with the spin labels was estimated and hence profiles of the local oxygen transport parameters across the membrane were obtained. The authors calculated the permeability for O_2 as the ratio of the permeability coefficient across the membrane to the permeability across the water layer, which is comparable with our calculation of permeability. The comparison of our calculated results with their experimental results is shown in Figure 10. We find that our result at 323 K is qualitatively consistent with their experimental results [31] at three lower temperatures. Since details of the structure for the membranes being studied here are only available at higher temperature (323 K) and phase changes can occur at lower temperatures, simulations at lower temperatures would not be realistic.

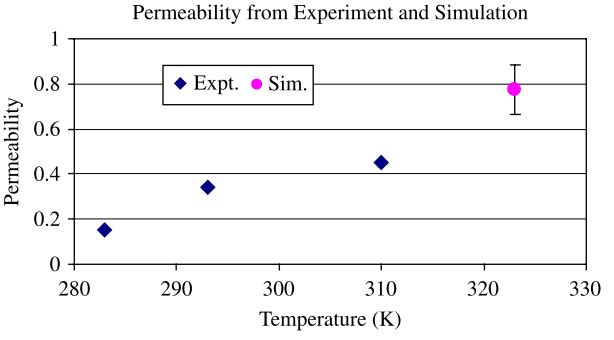

Figure 10. Comparison of permeability of oxygen in biomembrane (expt.) and our model membrane (sim.).

4. Conclusions

We have investigated gas permeation in several lipid bilayer systems using a CG model. By carefully designing our simulation system, we were able to measure the permeability of oxygen and xenon gases across the lipid bilayers DPPC, DMPC and DCPC. Our results showed satisfactory agreement with the experimental data where available.

Our study has shown that the MARTINI force field can successfully be used to simulate small molecule penetration into biomembranes and permeation across these membranes. We have also shown that the permeability expressed as the ratio of diffusion coefficients perpendicular and parallel to the lipid bilayer is a meaningful measure of gas permeability and permits direct comparisons with the experimental measurements. Further studies combined with NMR experimental measurements of the concentration profiles of the gas solute as a function of time in the aqueous phase outside the membrane, in the membrane and in the aqueous phase on the other side will clarify further the basic permeation process of small molecules across lipid bilayers, and we plan to conduct such studies in the future.

Acknowledgement

This research has been funded by a Department of Energy, Office of Basic Energy Science grant [Grant No. DE-FG02-08ER46538].

References

[1] E.A. Disalvo and S.A. Simon, *Permeability and Stability of Lipid Bilayers*, CRC Press, Boca Raton, FL, 1995.

[2] S.J. Marrink and H.J.C. Berendsen, *Simulation of water transport through a lipid membrane*, J. Phys. Chem. 98 (1994), pp. 4155–4168.

[3] A. Finkelstein, *Current Topics in Membranes and Transport*, Vol. 21, Academic Press, New York, 1984, pp. 295–308.

[4] S. Paula, A.G. Volkov, A.N. Van Hoek, T.H. Haines, and D.W. Deamer, *Permeation of protons, potassium ions, and small polar molecules through phospholipid bilayers as a function of membrane thickness*, Biophys. J. 70 (1996), pp. 339–348.

[5] M. Jansen and A. Blume, *A comparative study of diffusive and osmotic water permeation across bilayers composed of phospholipids with different head groups and fatty acyl chains*, Biophys. J. 68 (1995), pp. 997–1008.

[6] S.J. Marrink and H.J.C. Berendsen, *Permeation process of small molecules across lipid membranes studied by molecular dynamics simulations*, J. Phys. Chem. 100 (1996), pp. 16729–16738.

[7] D. Bemporad, C. Luttmann, and J.W. Essex, *Computer simulation of small molecule permeation across a lipid bilayer: dependence on bilayer properties and solute volume, size and cross-sectional area*, Biophys. J. 87 (2004), pp. 1–13.

[8] W. Shinoda, M. Mikami, T. Baba, and M. Hato, *Molecular dynamics study on the effects of chain branching on the physical properties of lipid bilayers: 2. Permeability*, J. Phys. Chem. B 108 (2004), pp. 9346–9356.

[9] T. Sugii, S. Takagi, and Y. Matsumoto, *A molecular-dynamics study of lipid bilayers: effects of the hydrogencarbon chain length on permeability*, J. Chem. Phys. 123 (2005), 184714-1–184714-8.

[10] Y. Wang, J. Cohen, W.F. Boron, K. Schulten, and E. Tajkhorshid, *Exploring gas permeability of cellular membranes and membrane channels with molecular dynamics*, J. Struct. Biol. 157 (2007), pp. 534–544.

[11] S.O. Nielsen, C.F. Lopez, G. Srinivas, and M.L. Klein, *Coarse grain models and the computer simulation of soft materials*, J. Phys. Condens. Mater. 16 (2004), pp. R481–R512.

[12] S.J. Marrink, A.H. de Vries, and A.E. Mark, *Coarse grained model for semiquantitative lipid simulations*, J. Phys. Chem. B 108 (2004), pp. 750–760.

[13] S.J. Marrink, H.J. Risselada, S. Yefimov, D.P. Tieleman, and A.H. de Vries, *The MARTINI force field: coarse grained model for biomolecular simulations*, J. Phys. Chem. B 111 (2007), pp. 7812–7824.

[14] L. Monticelli, S.K. Kandasamy, X. Periole, R.G. Larson, D.P. Tieleman, and S.J. Marrink, *The MARTINI coarse-grained force field: extension to proteins*, J. Chem. Theory Comput. 4 (2008), pp. 819–834.

[15] J.C. Shelley, M.Y. Shelley, R.C. Reeder, S. Bandyopadhyay, and M.L. Klein, *A coarse grain model for phospholipid simulations*, J. Phys. Chem. B 105 (2001), pp. 4464–4470.

[16] E.R. May, A. Narang, and D.I. Kopelevich, *Role of molecular tilt in thermal fluctuations of lipid membranes*, Phys. Rev. E 76(021913) (2007), pp. 1–6.

[17] R. Baron, A.H. de Vries, P.H. Hunenberger, and W.F. van Gunsteren, *Configurational entropies of lipids in pure and mixed bilayers from atomic level and coarse-grained molecular dynamics simulations*, J. Phys. Chem. B 110 (2006), pp. 15602–15614.

[18] M. Krishnamurthy, S. Murad, and J.D. Olson, *Molecular dynamics simulation of henry's constant of argon, nitrogen, methane and oxygen in ethylene oxide*, Mol. Simulat. 32 (2006), pp. 11–16.

[19] M. Bohn, S. Lago, J. Fischer, and F. Kohler, *Excess properties of liquid mixtures from perturbation theory: results for model systems and predictions for real systems*, Fluid Phase Equilibr. 23 (1985), pp. 137–151.

[20] J.G. Harris and K.H. Young, *Carbon dioxide's liquid–vapor coexistence curve and critical properties as predicted by a simple molecular model*, J. Phys. Chem. 99 (1995), pp. 12021–12024.

[21] G.C. Mitland, M. Rigby, E.B. Smith, and W.A. Wakeham, *Intermolecular Forces*, Oxford University Press, Oxford, 1981.

[22] S. Murad, K. Oder, and J. Lin, *Molecular simulation of osmosis, reverse osmosis, and elcetro-osmosis in aqueous and methanolic electrolyte solutions*, Mol. Phys. 95 (1998), pp. 401–408.

[23] K. Oder and S. Murad, *Molecular simulations of membrane based separations of supercritical electrolyte solutions*, Mol. Simulat. 25 (2000), pp. 229–238.

[24] S. Matysiak, C. Clementi, K. Kremer, and L.D. Site, *Modeling diffusive dynamics in adaptive resolution simulation of liquid water*, J. Chem. Phys. 128 (2008), 024503.

[25] LAMMPS (Large-scale Atomic/Molecular Massively Parallel Simulator), MD code developed by Steve Plimpton and co-workers at Sandia National Laboratories, DOE.

[26] J.F. Nagle and S. Tristram-Nagle, *Structure of lipid bilayers*, Biochim. Biophys. Acta. 1469 (2000), pp. 159–195.

[27] S. Nose, *A unified formulation of the constant temperature molecular dynamics methods*, J. Chem. Phys. 81 (1984), pp. 511–519.

[28] W.G. Hoover, *Canonical dynamics: equilibrium phase-space distributions*, Phys. Rev. A 31 (1985), pp. 1695–1697.

[29] H. Yuan, S. Murad, C.J. Jameson, and J.D. Olson, *Molecular dynamics simulations of Xe chemical shift and solubility in n-alkanes*, J. Phys. Chem. C 111 (2007), pp. 15771–15783.

[30] H. Yuan, C.J. Jameson, S.K. Gupta, J.D. Olson, and S. Murad, *Prediction of henry's constants of xenon in cyclo-alkanes from molecular dynamics simulations*, Fluid Phase Equilibr. 269 (2008), pp. 73–79.

[31] A. Tamimi, E.B. Rinker, and O.C. Sandall, *Diffusion coefficients for hydrogen sulfide, carbon dioxide, and nitrous oxide in water over the temperature range 293–368 K*, J. Chem. Eng. Data 39 (1994), pp. 330–332.

[32] W.K. Subczynski, L.E. Hopwood, and J.S. Hyde, *Is the mammalian cell plasma membrane a barrier to oxygen transport?*, J. Gen. Physiol. 100 (1992), pp. 69–87.

[33] T.X. Xiang and B.D. Anderson, *The relationship between permeant size and permeability in lipid bilayer membranes*, J. Membr. Biol. 140 (1994), pp. 111–122.

[34] J. Gutknecht, M.A. Bisson, and F.C. Tosteson, *Diffusion of carbon dioxide through lipid bilayer membranes: effects of carbonic anhydrase, bicarbonate, and unstirred layers*, J. Gen. Physiol. 69 (1977), pp. 779–794.

[35] M.P. Allen and D.J. Tildesley, *Computer Simulation of Liquids*, Oxford University Press, Oxford, 1989.

[36] S. Fishkoff and J.M. Vanderkooi, *Oxygen diffusion in biological and artifical membranes determined by the fluorochrome pyrene*, J. Gen. Physiol. 65 (1975), pp. 663–676.